References and Notes

1. T. A. Skotheim, Ed., *Handbook of Conducting Polymers* (Dekker, New York, 1986); H. S. Nalwa, Ed., *Handbook of Organic Conductive Molecules and Polymers* (Wiley, New York, 1997).
2. H. Naarmann and N. Theophilou, *Synth. Met.* **22**, 1 (1987).
3. J. Tsukamoto, A. Takahashi, K. Kawasaki, *Jpn. J. Appl. Phys.* **29**, 125 (1990).
4. I. Božović, *Mod. Phys. Lett. B* **1**, 81 (1987).
5. H. Shirakawa and S. Ikeda, *Polym. J.* **2**, 231 (1971).
6. K. Araya, A. Mukoh, T. Narahara, H. Shirakawa, *Chem. Lett.* (no. 7), 1141 (1984); *Synth. Met.* **14**, 199 (1986).
7. K. Akagi, H. Shirakawa, K. Araya, A. Mukoh, T. Narahara, *Polym. J.* **19**, 185 (1987).
8. K. Akagi *et al.*, *Synth. Met.* **17**, 241 (1987).
9. H. Shirakawa *et al.*, *J. Macromol. Sci. Chem.* **A25**, 643 (1988).
10. K. Akagi, M. Ito, S. Katayama, H. Shirakawa, K. Araya, *Mol. Cryst. Liq. Cryst.* **172**, 115 (1989).
11. K. Akagi, S. Katayama, M. Ito, H. Shirakawa, K. Araya, *Synth. Met.* **28**, D51 (1989).
12. The difference of $[\alpha]_D$ between (*R*)- and (*S*)-binol derivatives should be ascribed to an occurrence of partial racemization during the etherification reactions between the hydroxyl groups of the binaphthols and the PCH506 substituents. Because the boiling temperature of cyclohexanone, which was used as a reaction solvent, is 157°C, it is desirable that the etherification reaction be carried out by refluxing the cyclohexanone solution around 150°C. However, to obtain a higher yield, the reaction for the (*S*)-binol derivative was refluxed at 156°C, very close to the boiling point of cyclohexanone, and for longer times (22 hours) than in the case of the (*R*)-binol derivative (150°C and 14 hours). In fact, the yield (99.6%) of the (*S*)-binol derivative was higher than that (96.9%) of the (*R*)-binol derivative. However, more racemization during the etherification reaction seems to have occurred in the (*S*)-binol derivative than in the (*R*)-binol derivative.
13. Synthesis of the (*R*)-bino derivative shown in Scheme 3. K. Akagi, S. Kaneko, G. Piao, H. Shirakawa, M. Kyotani, unpublished results.
14. It is of keen interest that the hierarchical higher order structure observed in Fig. 5 resembles the helical self-assembled microstructure of such biological molecules as lipids. See J. M. Schnur, *Science* **262**, 1669 (1993), and references therein.

15. This research was supported by Grant-in-Aids for Scientific Research from the Japanese Ministry of Education, Culture and Science, and in part by the Tsukuba Advanced Research Alliance (TARA) project of the University of Tsukuba.

30 March 1998; accepted 26 October 1998

Macroscopic Quantum Interference from Atomic Tunnel Arrays

B. P. Anderson and M. A. Kasevich

Interference of atomic de Broglie waves tunneling from a vertical array of macroscopically populated traps has been observed. The traps were located in the antinodes of an optical standing wave and were loaded from a Bose-Einstein condensate. Tunneling was induced by acceleration due to gravity, and interference was observed as a train of falling pulses of atoms. In the limit of weak atomic interactions, the pulse frequency is determined by the gravitational potential energy difference between adjacent potential wells. The effect is closely related to the ac Josephson effect observed in superconducting electronic systems.

Josephson-effect interference experiments have become paradigms for understanding the physical manifestations of the phases of macroscopic quantum systems (*1, 2*). Bose-Einstein condensation in dilute alkali vapors (*3*) and recent interference studies with Bose-Einstein condensed atoms (*4*) raise the possibility of observing similar phase-dependent dynamics with dilute neutral-atom systems (*5*).

In the ac Josephson effect, application of a dc voltage, V, across a tunnel junction between two superconducting reservoirs leads to an alternating current through the junction with a frequency proportional to the applied voltage (*6*). The physical origin of the effect is the temporal interference of two macroscopic quantum states $|1\rangle$ and $|2\rangle$ of differing chemical potentials μ_1 and μ_2, respectively. The voltage-induced chemical potential difference between the states, $\mu_1 - \mu_2 = 2eV$, leads to a linear evolution of their relative quantum mechanical phase at a rate $(\mu_1 - \mu_2)/\hbar$ ($\hbar$ is Planck's constant, h, divided by 2π). This temporal phase slip results in an alternating current of frequency $2eV/\hbar$.

In our experiment, interference occurs between macroscopic quantum states comprising Bose-Einstein condensed atoms confined in an array of optical traps in a gravitational field. Neglecting atomic interactions, the chemical potential difference between adjacent traps is determined by the gravitational potential $U_G = mgz$, which is analogous to the applied voltage in the ac Josephson effect (m is the atomic mass, g the acceleration due to gravity, and z is the vertical coordinate). The traps are formed at the antinodes of a vertically oriented optical standing wave, which are separated by $\Delta z = \lambda/2$ (λ is the wavelength of light used to confine the atoms), and the chemical potential difference is $mg\lambda/2$. Coherent tunneling from these traps leads to a time-dependent atom current that is modulated at the frequency $\omega_J = mg\lambda/2\hbar$. This frequency depends only on fundamental constants, g, and the wavelength of the confining light.

A combined optical-plus-gravitational trapping potential similar to those used in this study is illustrated in Fig. 1. The quantum transport properties of periodic sloping potentials for single particles have been studied as models for electron motion under the influence of a static electric field in a crystal lattice (*7*). For weak external potential gradients, the external field can be treated as a perturbation to the band structure associated with the lattice. In this limit, wave packets remain confined in a single band and the external field drives coherent oscillations at the Bloch frequency (*8*). At higher field strengths, the field drives interband transitions to higher lying states, as first calculated by Zener in the context of dielectric breakdown in solids (*9*).

Our experimental parameters are in the regime where the bare lattice potential (neglecting the gravitational slope) supports only one band below its energy maximum. The width of this band is comparable to the gravitationally induced offset between adjacent wells of the combined potential. A single-particle eigenstate localizes over a small cluster of adjacent lattice sites (*10*). Particles that tunnel out of these states rapidly progress to a continuum state in which the lattice potential is a negligible perturbation on the gravitationally accelerated wave packet trajectories. The lattice states are populated in such a way that the wave function associated with the qth lattice position can be accurately described by the macroscopic state $\Psi_q = n_q^{1/2} e^{i\phi_q(t)}$. In the noninteracting limit, where effects due to interatomic collisions are negligible, the atom density n_q is determined by the single-particle wave function and the number of atoms, and the macroscopic phase $\phi_q(t)$ depends only on the initial phase at time $t = 0$ and the gravitational energy.

For appropriate experimental parameters, each lattice state can have a potentially significant tunneling probability into the (unbound) continuum and can be modeled as a point emitter of de Broglie waves with an emission rate proportional to the tunneling probability. The output from an array of such emitters localized at positions z_q^0 is obtained by summing over the coherent emission from each well. For an array of N traps the emission is

$$\Psi(z,t) = \sum_{q=1}^{N} A_q(t)\exp\left[i\int (k_q dz - \omega_q dt + \phi_q^0)\right] \quad (1)$$

where $\hbar k_q = m\sqrt{2g|z - z_q^0|}$ and $\hbar\omega_q =$

Physics Department, Yale University, New Haven, CT 06520, USA.

mgz_q^0 are the momentum and total energy associated with the gravitationally accelerated de Broglie wave, respectively (*11*). The coefficient A_q parameterizes both the tunneling time (emission rate) from the bound state to the continuum and the trap population (which changes slowly with time as the trap is depleted), and ϕ_q^0 is the initial relative phase between traps at time $t = 0$. The model assumes that the lattice has a negligible influence on the atoms once they are in the continuum.

Because the frequencies ω_q are equally spaced by an increment $\omega_J = mg\lambda/2\hbar$, we expect the detection probability $|\Psi|^2$ to be periodic with that frequency. The relative phases of the interfering components determine the detailed structure of the periodic atomic current. If the wells are initially populated with identical relative phases, as is the case in our experiment, the resulting probability distribution is a train of pulses (Fig. 2A). If the phases are randomly distributed (Fig. 2B), pulses no longer form. We confirmed the validity of the model in the noninteracting limit by comparing it with numerical solutions of the time-dependent Schrödinger equation, as shown in Fig. 2, C and D.

Pulse formation can be viewed equivalently as Zener tunneling at the turning point of a Bloch oscillation (*9*). Atoms confined in the lowest band oscillate at the Bloch frequency $mg\lambda/2\hbar$, identical to the Josephson frequency ω_J identified above. At the diffraction point in the Bloch cycle, the external field induces an interband transition to the continuum band, and a pulse is formed (*12*). The tunneling probability per oscillation, first calculated by Zener, is

$$P = \exp\left(-\frac{\lambda\epsilon^2}{8\hbar^2 g}\right) \quad (2)$$

where ϵ is the energy gap between the groundstate band and continuum states. Output pulses, then, are also signatures of an alternating atom current flowing between macroscopically populated lattice sites.

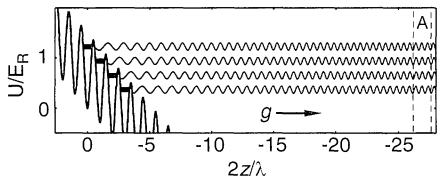

Fig. 1. The effective optical-plus-gravitational potential U/E_R for parameters used in our experiment ($E_R \equiv \hbar^2k^2/2m$ is the photon recoil energy with $k = 2\pi/\lambda$). The horizontal oscillating curves illustrate de Broglie waves from the tunnel output of each well. In region A, the relative phases of the waves interfere constructively to form a pulse. Heavy lines illustrate the energies of the lowest bound states of harmonic oscillator potentials that match the shapes of the actual potentials near each local energy minimum.

In our experimental approach, laser-cooled and trapped atoms were loaded into a magnetic trap and evaporatively cooled to temperatures below the Bose-Einstein condensation threshold. After condensing, atoms were transferred into the optical lattice and the magnetic trap was turned off. By adjusting the depth of the optical wells, we could control the tunneling rate from the wells so that it was fast enough to observe atoms leaving the traps, but slow enough to allow for direct observation of many periods of the temporally modulated signal described above before the traps were depleted.

The experimental apparatus (Fig. 3) has been described in detail elsewhere (*13*). Briefly, atoms were loaded into a magneto-optic trap (*14*) from a dilute ^{87}Rb vapor by established laser-cooling and trapping techniques (*15*). After a ~200-s loading interval, atoms were transferred into a magnetic time-averaged orbiting potential (TOP) trap (*16*) and were subsequently evaporatively cooled (*17*) by slowly reducing the trap depth and increasing the trap spring constants. A final radio frequency–induced evaporation stage was used to cool the atoms to condensation. We typically created condensates of $\sim 10^4$ atoms after ~30 s of evaporative cooling. After the phase transition, the magnetic trap spring constants were adiabatically reduced by a factor of 400 to 1000, enabling us to vary both the size and density of the condensate. The atoms were imaged with standard (destructive) absorptive imaging techniques: The shadow cast by a weak resonant probe laser beam, aligned to pass through the trapping region, was magnified and imaged onto a cooled slow-scan charge-coupled device (CCD) camera (Fig. 3). An image of a nearly pure Bose-Einstein condensate is shown in Fig. 4A.

The optical lattice traps were created by a standing wave of light whose wavelength $\lambda = 2\pi/k = 850$ nm was far detuned from the 780-nm Rb-cooling and trapping transitions (*18*). The effective potential from this laser field was $U_L \simeq U_L(x,y)\sin^2(kz)$, where $U_L(x,y)$ was determined by the transverse intensity profile of the (nearly Gaussian) laser beams (*19*). The $1/e^2$ radius of the transverse profile was ~80 μm, an order of magnitude larger than the transverse radius of the condensate. The well depths, which scale linearly with the intensity of the beam, could be controlled electronically with an acousto-optic modulator. At full intensity (~80 W/cm^2), the trap depths at the center of the beam were $2.1E_R$, where E_R is the recoil energy.

Atoms were transferred into the optical lattice from the magnetic trap by ramping up the intensity of the laser field (over 20 ms) while holding atoms in a weak magnetic trap. After this ramp, the magnetic quadrupole field was suddenly turned off. (The rotating magnetic field was left on to maintain the spin polarization of the sample.) The number of traps loaded (and the number of atoms in each trap) depended on the initial spatial extent of the condensate. For our parameters, about 30 wells were loaded. In recent related work, Stamper-Kurn *et al.* demonstrated confinement of Bose-Einstein condensed Na atoms in a far-detuned optical trap formed by a single, tightly focused, traveling-wave laser beam (*20*).

We measured the lifetime of the atoms confined in the lattice potential by recording images after various holding times. For a $2.1E_R$-deep lattice, the observed lifetime was ~50 ms. This loss is consistent with tunnel-

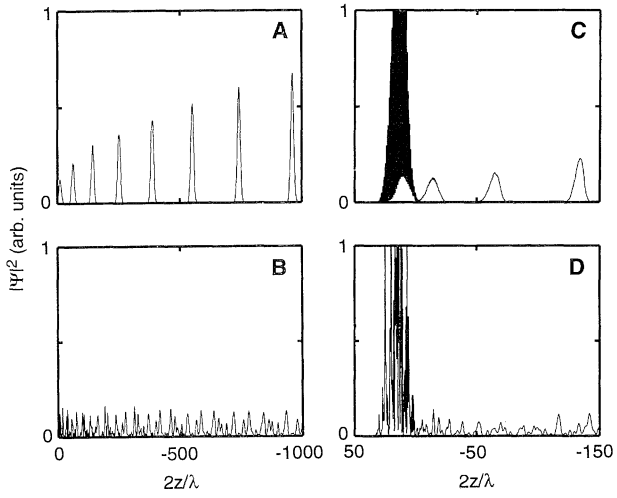

Fig. 2. (**A**) Model given by Eq. 1 for uniform initial phases, evaluated at $t = 10$ ms. The parameters $A_q(t)$ were taken to be independent of time (weak tunneling limit) and to have a Gaussian dependence on q (with a $1/e$ half-width of 15 wells). (**B**) Model given by Eq. 1 for random initial phases. (**C**) Numerical solution to the time-dependent Schrödinger equation showing the formation of pulses for the Hamiltonian $H = p^2/2m + U_L + U_G$ (p is the momentum operator). The initial state ($t = 0$) was approximated by a set of Gaussian wave packets. Each wave packet was initially localized at a lattice site, with a width determined by a harmonic approximation of the local potential minimum. The overall wave function amplitudes were scaled by a Gaussian envelope, and the initial phases for the wave functions were chosen to be identical. (**D**) Numerical solution for random initial phases. In (C) and (D), the large amplitude distribution near $z = 0$ shows the relative population confined in the lattice. This trapped distribution is not shown in (A) and (B).

ing loss calculated from Eq. 2 (for $\epsilon \sim E_R$) and also with numerical solutions to the time-dependent Schrödinger equation. The observed loss rate is much faster than the expected loss from off-resonant scattering of lattice photons or three-body collisions (*21*).

Faster tunneling rates were obtained by operating at a reduced optical intensity. Although these higher rates led to rapid depletion of the traps, they allowed for direct observation of the tunnel array output, as predicted in Eq. 1. This output is shown in Fig. 4, B to E, for a well depth of $1.4E_R$. We observed a train of pulses similar to the array output illustrated in Fig. 2, A and C. The pulse period obtained from the measured spatial separation of the pulses was 1.10 ± 0.05 ms, in good agreement with the expected value of 1.09 ms for $g = 9.8$ m/s^2. The measurement uncertainty arises in the spatial calibration of the imaging system. In our analysis, we assumed that the influence of the lattice potential on wave packet trajectories could be neglected after atoms had tunneled from the optical traps (verified numerically). Each pulse contained ~10^3 atoms. This corresponds to phase space densities per pulse that are well above the condition for quantum degeneracy (*22*). The tunneling rate could be increased by lowering the well depths, producing fewer pulses with more atoms per pulse. For example, well depths of $1.0E_R$ produced a train of about four pulses before the initially trapped population was depleted.

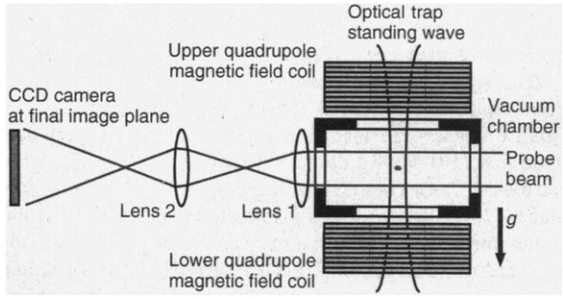

Fig. 3. Illustration of the apparatus. The ultrahigh vacuum chamber was designed to allow f/2.5 optical access through high-quality optical viewports attached to the chamber with indium metal seals. The quadrupole field coils for the magnetic trap are shown above and below the vacuum chamber. Not shown are the coils used to form the rotating field for the TOP trap and the laser beams used to initially laser cool and trap the atoms. A Bose-Einstein condensate was created at the center of the vacuum chamber and then loaded into the optical lattice. The spatial distribution of the atoms was imaged with a resonant, collimated, circularly polarized laser beam that was pulsed on through a window in the chamber and was incident on the atoms. The atoms absorbed light from the probe laser, leaving a shadow in the resulting probe beam intensity profile. This shadow was imaged onto a CCD camera with the illustrated optics. The absorption profile of the image was used to infer the atomic density profile. The probe beam was pulsed on when the rotating bias field was parallel with the propagation axis of the light. The measured resolution of the imaging system was 4.5 μm.

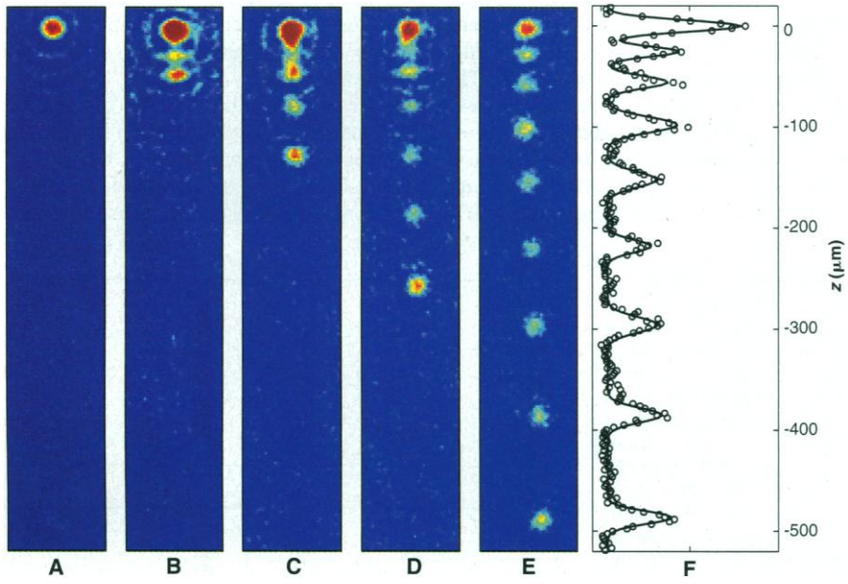

Fig. 4. (**A**) Absorption image of a Bose-Einstein condensate in a TOP trap. (**B** to **E**) Absorption images after fixed holding times in the optical lattice showing the time development of the pulse train; 3 ms (B), 5 ms (C), 7 ms (D), and 10 ms (E). Because the imaging process was destructive, a new condensate was created for each of these images. Pulses at the lower portion of the image were emitted at earlier times. The false-color scale is identical for (B) to (E) but was adjusted for (A) to avoid saturation. In images (B) to (E) the uppermost spot is an image of the lattice array, which overlaps with the last emitted pulse. The imaging resolution was not sufficient to resolve individual lattice sites. (**F**) The integrated absorption profile for (E), obtained by summing over the horizontal cross-sections. The solid black curve shows a nonlinear least squares fit to a series of Gaussian pulses constrained to be separated by a fixed time interval. The time between successive pulses can be inferred from their observed spatial separation. The measured intervals are (from the bottom to the top pulse) 1.13, 1.11, 1.09, 1.10, 1.05, 1.14, and 1.09 ms.

For high densities, we expect mean field interactions (*23*) to contribute to the chemical potential differences between adjacent lattice sites and potentially dephase the tunnel array output. The magnitude of this effect is estimated by calculating the interaction energies for the estimated particle densities in the lattice traps. At a peak density of $n_0 = 10^{13}$/cm^3, the mean field energy $U_{MF} = 4\pi\hbar^2 a n_0/m$ ($a = 5.5$ nm is the s-wave scattering length) is $k_B \cdot 4$ nK (k_B is the Boltzmann constant) per particle at the maximally populated well. For comparison, the kinetic energy per particle is $\sim E_R = k_B \cdot 157$ nK (*24*). The corresponding groundstate frequency shift due to the mean-field interaction is 80 Hz, whereas the maximum differential shift between adjacent wells is 4 Hz. Inclusion of shifts of these magnitudes in Eq. 1 shows that they are not large enough to dephase the pulse output during our observation time (10 ms). The effects of the mean-field interaction were controlled by changing the density of atoms in the trap. When we transferred at densities greater than 10^{13}/cm^3, we reached a regime where we observed a degradation in the interference.

The ac Josephson effect has played a key role in the determination of $2e/h$ and the volt by means of the Josephson voltage-frequency relation (*25*). High accuracy is obtained by converting voltage measurements into frequency measurements. One might expect similar gains in accuracy to be possible with atoms in, for example, the measurement of the strengths of weak forces. In our experiment, careful measurement of the pulse timing leads to precise determination of g. A nonlinear fit to the pulse train of Fig. 4E yields a value of $g = 9.6 \pm 0.4$ m/s^2, where the error is dominated by the systematic uncertainty in the imaging magnification. Use of a localized probe beam to detect individual pulses directly in the time domain would eliminate this uncertainty. The statistical error from the fit produces a resolution of $\delta g \sim 10^{-4} g$ after a 10-ms measurement time, or $\sim 10^{-5} g/\mathrm{Hz}^{1/2}$. Higher sensitivities could be achieved by increasing ω_J, which might be accomplished with a superlattice potential created from the interference of laser beams of differing frequencies to increase the spacing between adjacent wells (*26*).

Atomic analogs of Josephson effects could also be used in measurements of other

weak forces. For example, van der Waals–Casimir forces might be measured by interferometrically observing changes in the tunneling characteristics as the microtraps are brought near a surface. However, possible systematic shifts arising from mean-field interactions would need to be characterized.

Study of transport in a regime with strong nonlinearities induced by the mean-field interactions is an interesting problem in its own right, with ties to the problem of phase-locking in Josephson arrays (*27*) and the Bose-Hubbard model (*28*). These nonlinearities might be exploited to generate and study squeezed states of the atom field. We expect that relatively straightforward modifications of our experimental parameters should enable quantitative studies in this regime.

The tunnel array output can also be viewed as an atom laser (*29*) whose coherence length (>500 μm) greatly exceeds the dimensions of the resonator. The time-domain pulses are directly analogous to the output of a mode-locked laser source (*30*), in which interference occurs between many properly phased continuous-wave output beams. The nearly constant time interval between successive pulses directly implies that the relative phase associated with each pulse envelope is well defined.

References and Notes

1. B. D. Josephson, *Phys. Lett.* **1**, 251 (1962); P. Anderson, *Basic Notions of Condensed Matter Physics* (Benjamin/Cummings, Menlo Park, CA, 1984), and references therein.
2. For recent interference experiments with coupled superfluid ^{3}He resevoirs, see S. Pereverzev, A. Loshak, S. Backhaus, J. Davis, R. Packard, *Nature* **388**, 449 (1997); S. Backhaus, S. V. Pereverzev, A. Loshak, J. C. Davis, R. E. Packard, *Science* **278**, 1435 (1997).
3. M. H. Anderson, J. R. Ensher, M. R. Matthews, C. E. Wieman, E. A. Cornell, *Science* **269**, 198 (1995); K. Davis *et al.*, *Phys. Rev. Lett.* **75**, 3969 (1995); C. Bradley, C. Sackett, J. Tollett, R. Hulet, *ibid.*, p. 1687.
4. D. S. Hall, M. R. Matthews, C. E. Wieman, E. A. Cornell, abstract available at http://xxx.lanl.gov/abs/cond-mat/9805327; M. R. Andrews *et al.*, *Science* **275**, 637 (1997).
5. A. Smerzi, S. Fantoni, S. Giovanazzi, S. Shenoy, *Phys. Rev. Lett.* **57**, 3164 (1997); I. Zapata, F. Sols, A. Leggett, *Phys. Rev. A* **57**, R28 (1998).
6. See, for example, A. Barone and G. Paternó, *Physics and Applications of the Josephson Effect* (Wiley, New York, 1982).
7. See, for example, J. Callaway, *Quantum Theory of the Solid State* (Academic Press, New York, ed. 2, 1991).
8. S. Wilkinson, C. Bharucha, K. Madison, Q. Niu, M. Raizen, *Phys. Rev. Lett.* **76**, 4512 (1996); Q. Niu, X. Zhao, G. A. Georgakis, M. Raizen, *ibid.*, p. 4504; M. Dahan, E. Peik, J. Reichel, Y. Castin, C. Salomon, *ibid.*, p. 4508.
9. C. Zener, *Proc. R. Soc. London Ser. A* **145**, 523 (1934).
10. Formally, the eigenstates are the Wannier-Stark states ψ_p, which are linear superpositions of the localized tight-binding (Wannier) states w_q: $\psi_p = \Sigma_q J_{q-p}(4T/mg\lambda)w_q$. Here J_n is the nth-order Bessel function, and T is the tunneling matrix element between lattice sites. See, G. Wannier, *Phys. Rev.* **117**, 432 (1961); H. Fukuyama, R. Bari, H. Fogedby, *Phys. Rev. B* **8**, 5579 (1973); D. Emin and C. Hart, *ibid.* **36**, 7353 (1987).
11. In this model, the position z_q^0 is offset by an arbitrary factor from the local lattice minimum. Because this offset is identical for each well, it amounts to a trivial spatial shift in the interference pattern.
12. Numerical solutions to the nonlinear Schrödinger equation indicate an oscillation amplitude of a few lattice sites for parameters used in our experiments.
13. B. Anderson and M. Kasevich, *Phys. Rev. A.*, in press.
14. E. Raab, M. Prentiss, A. Cable, S. Chu, D. Pritchard, *Phys. Rev. Lett.* **59**, 2631 (1987).
15. S. Chu, L. Hollberg, J. Bjorkholm, A. Cable, A. Ashkin, *ibid.* **58**, 48 (1985); P. Lett *et al.*, *ibid.* **61**, 169 (1988); J. Dalibard and C. Cohen-Tannoudji, *J. Opt. Soc. Am. B* **6**, 2023 (1989); P. Ungar, D. Weiss, E. Riis, S. Chu, *ibid.*, p. 2058.
16. W. Petrich, M. Anderson, J. Ensher, E. Cornell, *Phys. Rev. Lett.* **74**, 3352 (1995).
17. N. Masuhara *et al.*, *ibid.* **61**, 935 (1988).
18. B. Anderson, T. Gustavson, M. Kasevich, *Phys. Rev. A* **53**, R3727 (1996). See also, S. Friebel, C. D'Andrea, J. Walz, M. Weitz, T. Hänsch, *ibid.* **57**, R20 (1998); T. Müller-Seydlitz *et al.*, *Phys. Rev. Lett.* **78**, 1038 (1997).
19. See, for example, J. Gordon and A. Ashkin, *Phys. Rev. A* **21**, 1606 (1980). In the far-detuned limit, the potential is $\hbar\Omega_r^2/\Delta$, where Ω_r is the transition Rabi frequency and Δ is the detuning.
20. D. Stamper-Kurn *et al.*, *Phys. Rev. Lett.* **80**, 2027 (1998).
21. At our operating parameters, the photon scattering rate was <0.01 photon/s. From the probe absorption we infer a peak trap density of $\sim 10^{13}$ atoms/cm^3. Using the three-body loss coefficient from P. Fedichev, M. Reynolds, G. Shlyapnikov, *Phys. Rev. Lett.* **77**, 2921 (1996), we estimate a collision time of $\sim 4 \times 10^3$ s.
22. Phase space density is $n\lambda_{th}^3$, where $\lambda_{th} = \sqrt{2\pi\hbar^2/mk_BT}$ is the thermal de Broglie wavelength. Quantum degeneracy is realized for $n\lambda_{th}^3 > 1$. We inferred the temperature, T, from the spatial expansion of a pulse during the observation interval, and density, n, from the observed optical depth and spatial extent of the pulse (Fig. 4).
23. See, for example, G. Baym and C. Pethick, *Phys. Rev. Lett.* **76**, 6 (1996).
24. Note that turning on the optical potential adiabatically takes the condensate from the Thomas-Fermi regime (lattice potential off), where mean-field interaction energy dominates kinetic energy, to a regime where kinetic energy dominates the mean-field energy (lattice potential on).
25. See, for example, B. Taylor, W. Parker, D. Langenberg, *Rev. Mod. Phys.* **41**, 375 (1969).
26. For example, 10^7 atoms confined to a lattice with a 100-μm period would yield an acceleration sensitivity of $\sim 10^{-13}g$, assuming the atoms initially populate 10 wells and are observed to tunnel over a 100-s interval.
27. A. Jain, K. Likharev, J. Lukens, J. Sauvageau, *Phys. Rep.* **109**, 309 (1984).
28. D. Jaksh, C. Bruder, J. I. Cirac, C. W. Gardiner, P. Zoller, http://xxx.lanl.gov/abs/cond-mat/9805329.
29. M. Mewes *et al.*, *Phys. Rev. Lett.* **78**, 582 (1997).
30. A. Siegman, *Lasers* (University Science Books, Mill Valley, CA, 1986).

31. We thank M. Yasuda for technical assistance. Supported by the NSF and the Office of Naval Research.

13 August 1998; accepted 30 September 1998

Viscoelastic Flow in the Lower Crust after the 1992 Landers, California, Earthquake

Jishu Deng,* Michael Gurnis, Hiroo Kanamori, Egill Hauksson

Space geodesy showed that broad-scale postseismic deformation occurred after the 1992 Landers earthquake. Three-dimensional modeling shows that afterslip can only explain one horizontal component of the postseismic deformation, whereas viscoelastic flow can explain the horizontal and near-vertical displacements. The viscosity of a weak, about 10-km-thick layer, in the lower crust beneath the rupture zone that controls the rebound is about 10^{18} pascal seconds. The viscoelastic behavior of the lower crust may help to explain the extensional structures observed in the Basin and Range province and it may be used for the analysis of earthquake hazard.

The Landers M_w 7.3 earthquake is dominated by right-lateral strike-slip shear along four major multibranched fault segments (*1*) (Fig. 1A). Previous observations showed that postseismic deformation occurred in the local pull-apart basins or compressive jogs where two or more branches intersect on the surface (*2*). The local deformation within these fault structures can be explained by a time-dependent change in fluid pore pressure (*2*, *3*).

In addition to the fault-localized postseismic effects, broad-scale (for example about one to several fault lengths) postseismic deformation following the Landers earthquake has been observed by the global positioning system (GPS) and interferometric synthetic aperture radar (InSAR) measurements (*4*–*8*). The northern part of the earthquake rupture along the Emerson fault, moved in the horizontal direction perpendicular to the fault trace (fault-normal direction) for tens of millimeters (*4*) to the southwest. The GPS measurements (*4*) and InSAR images (*5*) also constrain postseismic rebound in the horizontal fault-parallel and near-vertical satellite line-of-sight (LOS) directions. Whether this broad-scale time-dependent rebound is driven by continuous afterslip below seismogenic depth on the fault plane (*4*, *8*, *9*) or by viscoelastic flow in the lower crust in response to the coseismic stress concentration (*10*–*13*) is not well understood. Savage (*14*) demonstrated the difficulty of distinguishing

Seismological Laboratory 252-21, California Institute of Technology, Pasadena, CA 91125, USA.

*To whom correspondence should be addressed. E-mail: jishu@gps.caltech.edu